Article

Molecular Cell

R-Loop Mediated *trans* Action of the *APOLO* Long Noncoding RNA

Graphical Abstract

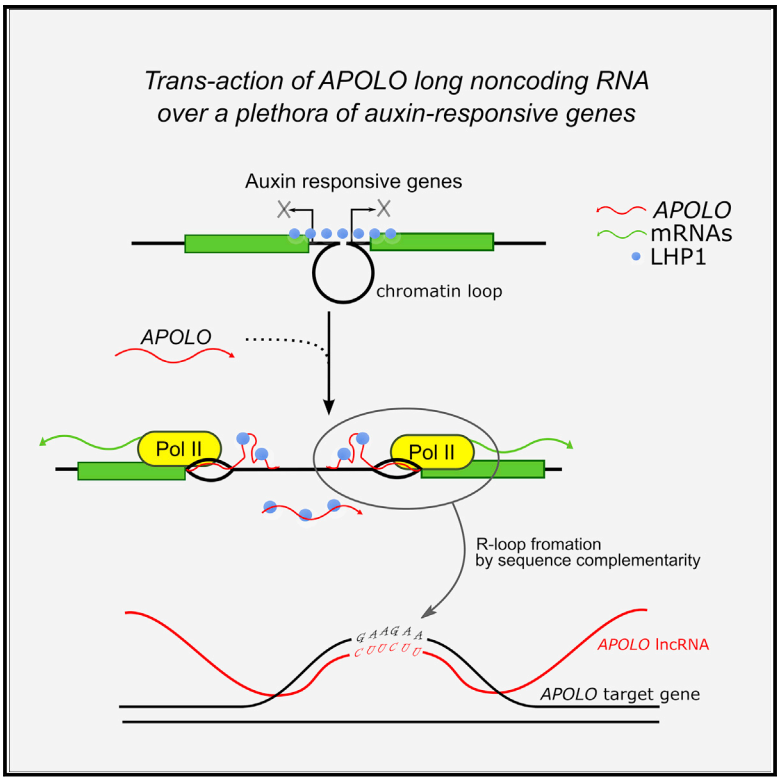

Authors

Federico Ariel, Leandro Lucero, Aurelie Christ, ..., Chang Liu, Moussa Benhamed, Martin Crespi

Correspondence

fariel@santafe-conicet.gov.ar (F.A.), martin.crespi@ips2.universite-paris-saclay.fr (M.C.)

In Brief

In this work, Ariel et al. demonstrated that the *APOLO* long noncoding RNA can coordinate expression of multiple genes through sequence complementarity and R-loop formation in plants. Upon target recognition, *APOLO* can decoy protein complexes and modulate the three-dimensional chromatin conformation to fine-tune gene transcription.

Highlights

- Long noncoding RNAs modulate chromatin three-dimensional conformation in nuclei
- Target recognition in *trans* by long noncoding RNAs can be mediated by R-loop formation
- Through R-loop formation, noncoding RNAs can decoy Polycomb proteins from chromatin
- R-loops mechanisms may determine regulation of multiple genes by non-coding RNAs

Ariel et al., 2020, Molecular Cell *77*, 1055–1065
March 5, 2020
https://doi.org/10.1016/j.molcel.2019.12.015

CellPress

Molecular Cell
Article

R-Loop Mediated *trans* Action of the *APOLO* Long Noncoding RNA

Federico Ariel,[1,2,8,*] Leandro Lucero,[2,5] Aurelie Christ,[1,5] Maria Florencia Mammarella,[2] Teddy Jegu,[1,6,7] Alaguraj Veluchamy,[3] Kiruthiga Mariappan,[3] David Latrasse,[1] Thomas Blein,[1] Chang Liu,[4] Moussa Benhamed,[1] and Martin Crespi[1,*]

[1]Institute of Plant Sciences Paris-Saclay (IPS2), CNRS, INRA, Universities Paris-Sud, Evry and Paris-Diderot, Sorbonne Paris-Cite, University of Paris-Saclay, Batiment 630, 91405 Orsay, France
[2]Instituto de Agrobiotecnología del Litoral, CONICET, FBCB, Universidad Nacional del Litoral, Colectora Ruta Nacional 168 km 0, 3000 Santa Fe, Argentina
[3]Division of Biological and Environmental Sciences and Engineering, King Abdullah University of Science and Technology, Thuwal 23955-6900, Kingdom of Saudi Arabia
[4]Department of General Genetics, Center for Plant Molecular Biology (ZMBP), University of Tübingen, Auf der Morgenstelle 32, 72076 Tübingen, Germany
[5]These authors contributed equally
[6]Present address: Howard Hughes Medical Institute, Department of Molecular Biology, Massachusetts General Hospital, Boston, MA 02114, USA
[7]Present address: Department of Genetics, Harvard Medical School, Boston, MA 02114, USA
[8]Lead Contact
*Correspondence: fariel@santafe-conicet.gov.ar (F.A.), martin.crespi@ips2.universite-paris-saclay.fr (M.C.)
https://doi.org/10.1016/j.molcel.2019.12.015

SUMMARY

In eukaryotes, three-dimensional genome organization is critical for transcriptional regulation of gene expression. Long noncoding RNAs (lncRNAs) can modulate chromatin conformation of spatially related genomic locations within the nucleus. Here, we show that the lncRNA *APOLO* (*AUXIN-REGULATED PROMOTER LOOP*) recognizes multiple distant independent loci in the *Arabidopsis thaliana* genome. We found that *APOLO* targets are not spatially associated in the nucleus and that *APOLO* recognizes its targets by short sequence complementarity and the formation of DNA-RNA duplexes (R-loops). The invasion of *APOLO* to the target DNA decoys the plant Polycomb Repressive Complex 1 component LHP1, modulating local chromatin 3D conformation. *APOLO* lncRNA coordinates the expression of distal unrelated auxin-responsive genes during lateral root development in *Arabidopsis*. Hence, R-loop formation and chromatin protein decoy mediate *trans* action of lncRNAs on distant loci.

INTRODUCTION

The three-dimensional organization of genomes is critical for transcriptional regulation of gene expression and development of higher organisms. Increasing evidence shows that long noncoding RNAs (lncRNAs) participate in nuclear organization. They have been linked to the assembly and maintenance of nuclear domains through active transcription and recruitment of interacting proteins. LncRNAs can modulate chromatin conformation in *cis*, and also in *trans*, when distal genomic locations are brought into close spatial proximity within the nucleus (Simon et al., 2011; Maass et al., 2012; Engreitz et al., 2013; Hacisuleyman et al., 2014; Quinodoz and Guttman, 2014; Rinn and Guttman, 2014; West et al., 2014; Cloutier et al., 2016; Jégu et al., 2017). Here, we show a novel mechanism by which the lncRNA *APOLO* (*AUXIN REGULATED PROMOTER LOOP*) is able to recognize multiple distant independent loci in the *Arabidopsis thaliana* genome. By combining chromatin isolation by RNA purification followed by sequencing (ChIRP-seq) and RNA sequencing (RNA-seq), we identified a subset of *bona fide APOLO* targets across the *Arabidopsis* genome. Using genome-wide chromatin conformation capture, HiC, we found that these loci are apparently not spatially associated in the nucleus, challenging the concept of a distance-based restriction for lncRNA action. Interestingly, our findings indicate that *APOLO* recognizes its multiple independent targets by sequence complementarity and the formation of DNA-RNA duplexes (R-loops). Modulating *APOLO* RNA levels affects R-loop formation, chromatin 3D conformation, and the transcriptional activity of these distal loci, including a subset of auxin-responsive genes, to coordinate their expression during lateral root formation in *Arabidopsis*. The invasion of *APOLO* to the target DNA double strand decoys the plant Polycomb Repressive Complex 1 component LHP1 from these loci and induces their coordinated regulation. Altogether, our results indicate that R-loop formation and chromatin protein decoy are mediators of the *trans* action of lncRNAs.

RESULTS

It was previously shown that *APOLO* noncoding transcription dynamically modulates the formation of a chromatin loop in *cis*

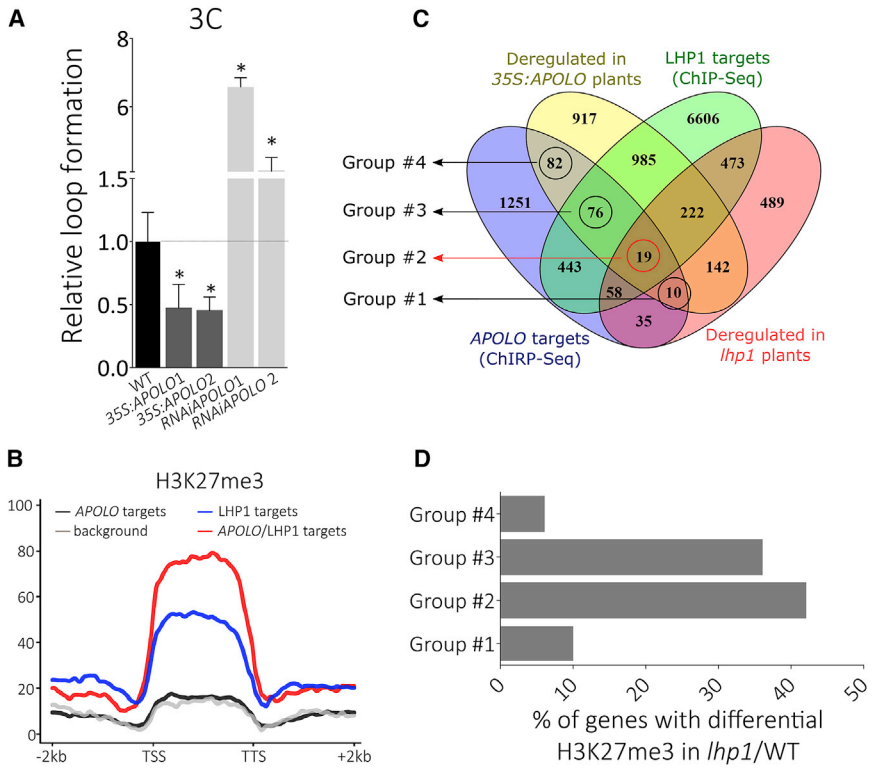

Figure 1. *APOLO* Recognizes Multiple Loci in *trans* across the *Arabidopsis* Genome

(A) Relative loop formation between *APOLO* and *PID* measured by 3C-qPCR in WT plants compared to two independent lines of *APOLO* overexpressing (35S promoter) and knockdown (RNAi) lines. Asterisks (*) indicate t test < 0.05.

(B) H3K27me3 distribution pattern (tag density) over the gene body and flanking regions for all *Arabidopsis* genes (grey), all putative *APOLO* targets (black), all LHP1 targets (blue), and the subset of common *APOLO*/LHP1 targets (red). TSS, transcription start site; TTS, transcription termination site. The metagene plot was generated using the R program.

(C) Venn diagram of genes targeted by *APOLO* (*APOLO*-ChIRP), deregulated in the *35S:APOLO* plants (*35S:APOLO* up/down), LHP1 targets (LHP1-ChIP), and genes deregulated in the *lhp1* mutant plants. *Bona fide* targets (*35S:APOLO*/*APOLO*-ChIRP intersection) are sub-classified into four groups. Group 1, 10 genes; group 2, 19 genes (red circle); group 3, 76 genes; and group 4, 82 genes.

(D) Percentage of differential H3K27me3 deposition in *lhp1* vs WT plants for groups 1–4, further described in Figure S1D.

See also Figure S1 and Tables S1 and S2.

between its own locus and its neighboring gene *PID*, fine-tuning its transcriptional activity. *APOLO* knockdown by RNAi resulted in enhanced formation of a local chromatin loop (Ariel et al., 2014). Strikingly, when we expressed *APOLO* under the control of the constitutive promoter *35S* in transgenic *Arabidopsis* plants, thus in another genomic location, the formation of the chromatin loop of the endogenous *PID-APOLO* region was impaired (Figure 1A), indicating that the *APOLO* RNA can recognize its own locus in *trans*. This was likely not due to transgene crossed silencing of the endogenous locus because *APOLO* RNA was highly expressed in these lines (Figure S1A). Therefore, we decided to perform a chromatin isolation by *APOLO*-RNA purification followed by DNA-seq (*APOLO* ChIRP-seq) to identify potential distant targets of the endogenous *APOLO* lncRNA in wild type (WT) plants. As a result, we obtained a list of 1,974 potential *APOLO* targets (Table S1), recognized in two independent ChIRP samples (using ODD and EVEN sets of probes), and undetected in the negative control (using probes against *LacZ* RNA). Moreover, as basal *APOLO* transcript levels are very low, we performed an RNA-seq experiment comparing WT and *35S:APOLO* plants to assess the effect of *APOLO* accumulation over the *Arabidopsis* transcriptome. We identified 2,468 differentially expressed genes (Table S2). Crossing both datasets, only 187 genes were common, suggesting that they are sites of direct regulation, and we called them *bona fide APOLO* targets (Table S3A). We focused on this subset of genes for further studies, to avoid potential false positives of the *APOLO* ChIRP-seq. From these 187 genes, 76% were transcriptionally up-regulated in the *APOLO* over-expressing plants (Figure S1B) whereas the others were down-regulated. The plant PRC1 protein LHP1 can interact with RNAs *in vitro* (Berry et al., 2017), including direct recognition of *APOLO in vivo* (Ariel et al., 2014). Considering that LHP1 recognizes the repressive mark H3K27me3 (Turck et al., 2007), we assessed the distribution of this histone modification over the gene body of all *APOLO* potential targets, LHP1 targets, and genes exhibiting both *APOLO* and LHP1 signatures. As expected, the H3K27me3 mark is enriched for LHP1 targets, but this mark is even higher for both *APOLO*/LHP1 targets (Figure 1B). This significant enrichment in H3K27me3 over common targets hints at the existence of characteristic features of each subset of *APOLO*-regulated genes. Thus, we sub-classified the 187 *APOLO bona fide* targets into four groups, according to LHP1 occupancy and their transcriptional behavior in the *lhp1* mutant versus WT plants (Veluchamy et al., 2016) (Figure 1C). Remarkably, group 2 and group 3 *APOLO bona fide* targets are enriched in genes with altered H3K27me3 deposition in the *lhp1* mutants (Veluchamy et al., 2016), compared to groups 1 and 4 (Figures 1D and S1C–S1H). Therefore, *APOLO* and LHP1 targets can be sub-classified according to their epigenetic landscape and their transcriptional behavior in *35S:APOLO* and *lhp1* plants.

Interestingly, among the 187 *bona fide APOLO* targets we found *WAG2* (in group 3), a gene encoding a kinase involved in auxin transport, homolog to the *APOLO* neighboring gene *PID* (Dhonukshe et al., 2015) (Figure 2A) although very distant in the genome. *WAG2* transcripts are augmented in the *35S:APOLO* lines and repressed in the RNAi plants both in control conditions and in response to auxin (Figure 2C). According to the *Dpn*II-based HiC dataset (Liu et al., 2016), a chromatin loop of approximately 12 kb exists between *WAG2* and the gene At3g14400,

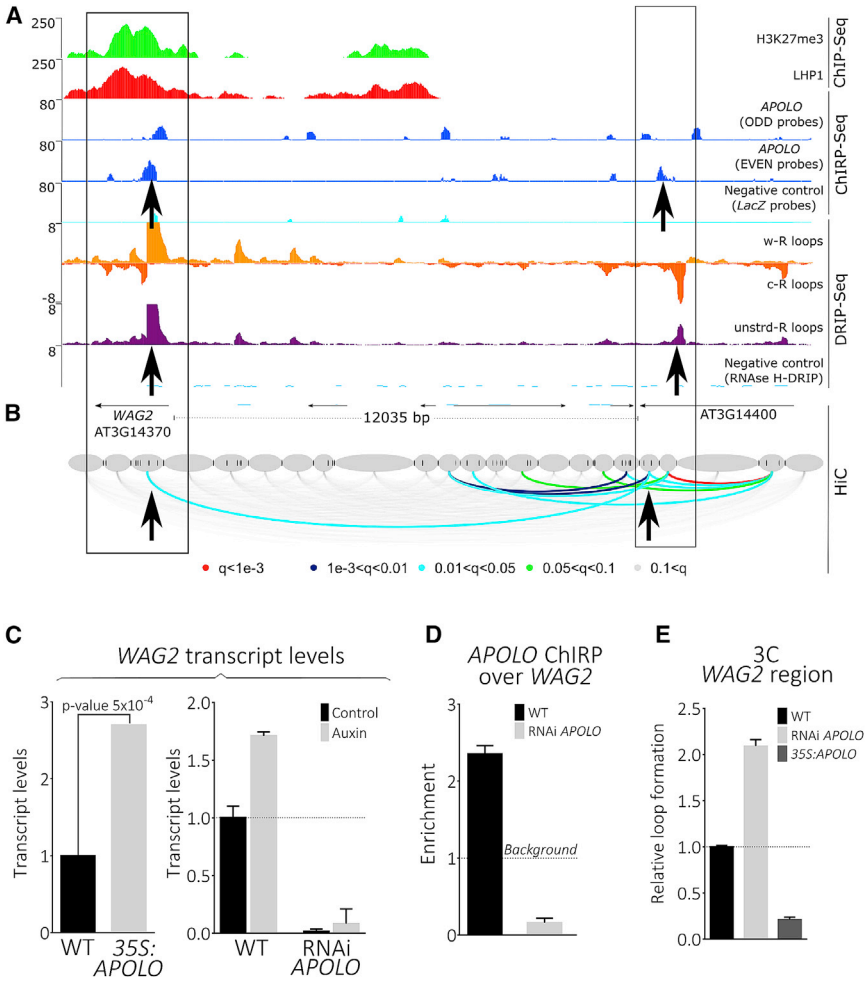

Figure 2. *APOLO* Directly Regulates the *WAG2* Locus in *trans*

(A) Epigenomic landscape of the *WAG2* locus. Lane 1: H3K27me3 deposition by ChIP-seq (Veluchamy et al., 2016). Lane 2: LHP1 deposition by ChIP-seq (Veluchamy et al., 2016). Lanes 3–5: *APOLO* recognition by ChIRP-seq (lanes 3 and 4, using ODD and EVEN sets of probes against *APOLO*, respectively; lane 5, negative control using LacZ probes). Lanes 6–9: R-loop formation by DRIP-seq (Xu et al., 2017), on Watson strand (lane 6), Crick strand (lane 7), or unstranded sequencing (lane 8). DRIP negative control after RNAseH treatment is shown in lane 9. Gene annotation is shown at the bottom.

(B) Chromatin loops identified in the *WAG2* region by *Dpn*II HiC (Liu et al., 2016). Colors of the loops are related to the corresponding q values indicated below. Black arrows in (D) and (E) indicate the same genomic locations, where the bases of the chromatin loop correlate with R-loop formation and *APOLO* recognition.

(C) Relative *WAG* transcript levels measured by qRT-PCR in WT plants vs *35S:APOLO* plants and in *APOLO* RNAi (in control conditions and in response to NPA-NAA treatment, Auxin).

(D) Validation of *APOLO* binding to the *WAG2* locus by ChIRP-qPCR in WT and *APOLO* RNAi plants. The mean of ODD and EVEN probes ChIRP-qPCR is expressed (value 1 is background level, defined by LacZ probes ChIRP).

(E) Relative formation of the loop indicated in (B), measured by 3C-qPCR in WT plants vs *APOLO* RNAi and *35S:APOLO* plants. The bars show the SD of the corresponding number of independent biological replicates.

encompassing the *WAG2* promoter and four additional genes (Figure 2B). Therefore, we first confirmed the *APOLO* RNA-*WAG2* DNA interaction by ChIRP-qPCR on WT versus *APOLO* RNAi plants (Figure 2D). Then, we quantified the relative loop formation in *APOLO* knockdown (RNAi) and *35S:APOLO* plants versus WT, exhibiting an enhanced and an impaired formation, respectively (Figure 2E). Altogether, our results indicate that *APOLO* lncRNA regulates two homolog genes: its neighboring gene *PID* in *cis*, as well as *WAG2* in *trans*, by affecting both local chromatin loop formation and the transcriptional activity of each of them.

Considering that *APOLO* is transcriptionally modulated by auxin (Ariel et al., 2014) and that *WAG2* and *PID* are involved in auxin transport (Armengot et al., 2016), we wondered to what extent *APOLO* is capable of directly co-regulating auxin-related genes during development. Thus, we first assessed the enrichment of auxin-responsive genes among the *APOLO bona fide* targets as well as among all genes deregulated in the *35S:APOLO* plants. To this end, we performed a hypergeometric analysis of each list compared to the one of auxin-responsive genes determined by RNA-seq (Bazin et al., 2018). *APOLO bona fide* targets are significantly enriched in auxin-responsive genes (71 genes out of 187, $p = 1.1 \times 10^{-5}$). Moreover, the enrichment is remarkably higher for genes deregulated in the *35S:APOLO* plants (888 genes out of 2,415, $p = 8.2 \times 10^{-241}$), suggesting that *APOLO* directly regulates a subset of key genes that will modulate the global auxin-responsive transcriptome (Figure S2A). Then, we expressed in transgenic plants the full *PID-APOLO* intergenic region (*ProAPOLO*) controlling the reporter genes *GFP-GUS* (Figure S2D). These plants were crossed with those transformed with the synthetic auxin-responsive promoter *DR5* directing the expression of *erRFP* (Marin et al., 2010) in maximal auxin response peaks. GUS staining revealed that *APOLO* promoter is active during lateral root (LR) development (Figure 3A), a process governed by auxin (Lavenus et al., 2013). Before LR initiation, *APOLO* is expressed in pericycle cells. Progressively during LR development (Malamy and Benfey, 1997), the *APOLO* promoter activity is restricted at the base of the primordium (Figure 3A), as confirmed by confocal observation of GFP (Figures 3B and S2E). In the apex of the emerged LR, *ProAPOLO* is active in outer layers of columella cells (in green; Figure 3C), whereas the peak of auxin response was identified in the quiescent center and the inner layer of columella cells (in red). In order to decipher the function of *APOLO* during LR development, we analyzed the Gene Ontology of the 187 *bona fide* targets. Enrichment was found for categories

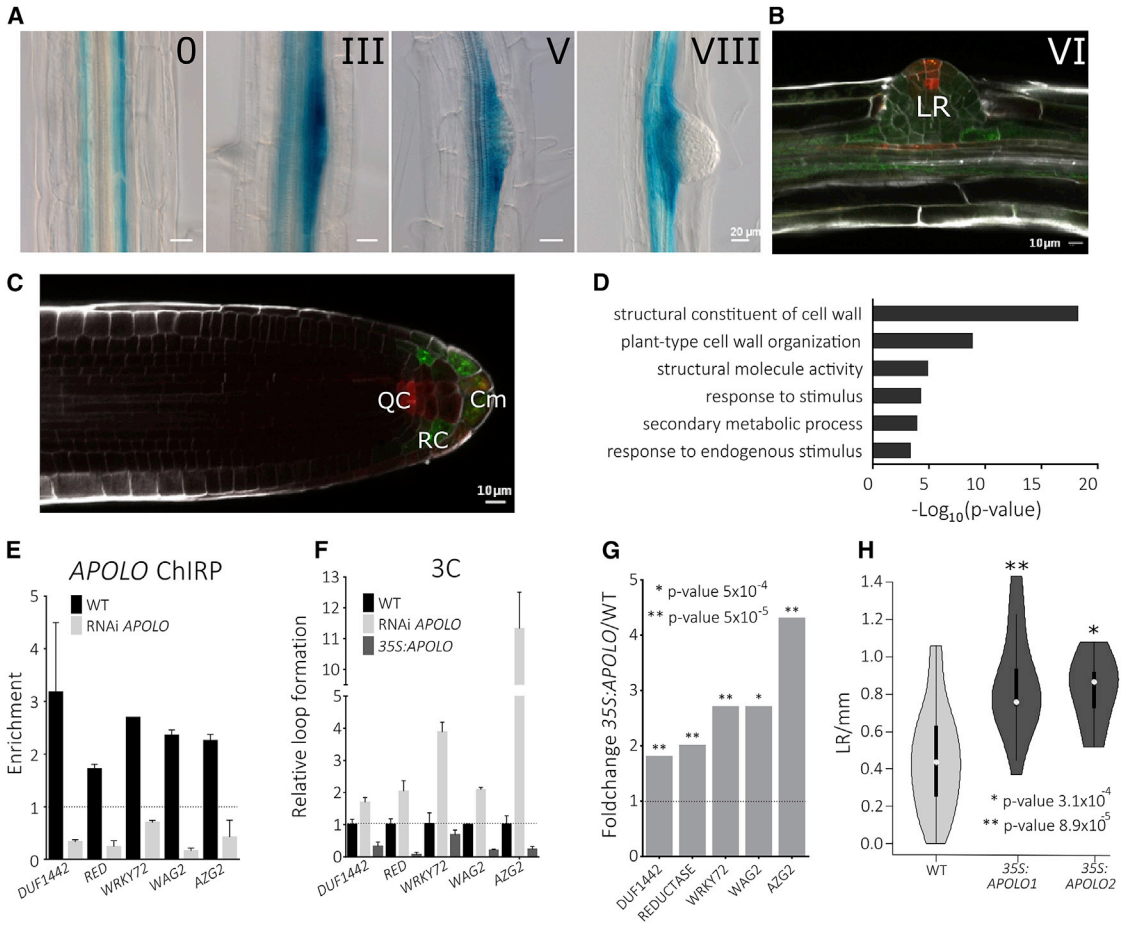

Figure 3. *APOLO* Regulates Lateral Root Formation by Co-modulating Chromatin Conformation of Multiple Auxin-Responsive Genes

(A) GUS staining showing *APOLO* promoter activity during lateral root (LR) formation.

(B) Confocal visualization of *ProAPOLO:erGFP* and *DR5:erRFP* on a LR primordium. *ProAPOLO* is active at the base of the primordium whereas the auxin peak has place in the LR forming meristem. In (A) and (B), the numbers O to VIII refer to the LR developmental stage according to Malamy and Benfey (1997).

(C) Confocal observation of the emerged LR apex. The activity of *ProAPOLO* in the external cells of the columella (Cm) and the root cap (RC) cells is shown in green (*erGFP*), whereas the auxin maximum is indicated in red (*DR5:erRFP*), in the quiescent center (QC) and the inner layers (initials) of columella cells. Co-localization of *DR5* and *ProAPOLO* activity is observed in the outer layer of columella cells.

(D) Gene Ontology analysis of the 187 *bona fide APOLO* targets. Bars express the $-\log_{10}$(p value) of the corresponding enrichment categories.

(E) *APOLO* association to DNA of selected genomic targets by ChIRP-qPCR in WT and RNAi plants. The dotted line shows the background, as for Figure 1G.

(F) Relative chromatin loop formation by 3C-qPCR deduced from the HiC dataset (Liu et al., 2016), in WT plants vs *35S:APOLO* and RNAi lines for selected targets. The dotted line indicates loop formation detected in WT plants by qPCR, taken as 100%.

(G) Transcript levels of the subset of genes analyzed in (F) and (G), quantified from the RNA-seq in WT vs *35S:APOLO* plants.

(H) Violin plots of the lateral root density of WT plants and the two independent *35S:APOLO* lines. 50 individuals were analyzed for WT, 14 for *35S:APOLO1*, and 8 for *35S:APOLO2*. White circles indicate the median and colored shapes indicate the probability distribution of the data. The bars show the SD of the corresponding number of independent biological replicates.

See also Figures S2 and S3 and Table S3.

related to cell wall composition and organization (Figure 3D). In particular, we identified among *APOLO* targets three genes coding for EXTENSIN proteins (in group 2), one of which, *LEUCINE RICH EXTENSIN2 (LRX2)*, promotes cell wall remodeling during LR formation (Lewis et al., 2013). Furthermore, the VisuaLRTC database (Lateral Root Compendium; Parizot et al., 2010), linking genes to LR initiation (*solitary root* (*slr*)-dependent auxin regulation) or LR development (*auxin response factor* (*arf*)*7* and/or *arf19*-dependent auxin regulation), allowed us to associate *APOLO* auxin-responsive *bona fide* targets to each stage of LR formation (Table S3C). Particularly, a higher number of genes from the four groups were involved in ARF-dependent LR development rather than LR initiation (Figure S2B). According to the VisuaLRTC (Parizot et al., 2010), the transcriptional response of *PID* to exogenous auxin is dependent on the *ARF7* and *19* (Ariel et al., 2014). Considering that two putative ARF *cis*-acting elements are present in the intergenic region between *PID* and *APOLO* (Figure S2D), we made use of *arf7-arf19* double mutants complemented with a PRO_{ARF7}*:ARF7* construction tagged with the glucocorticoid-receptor *GR* (Lavenus et al.,

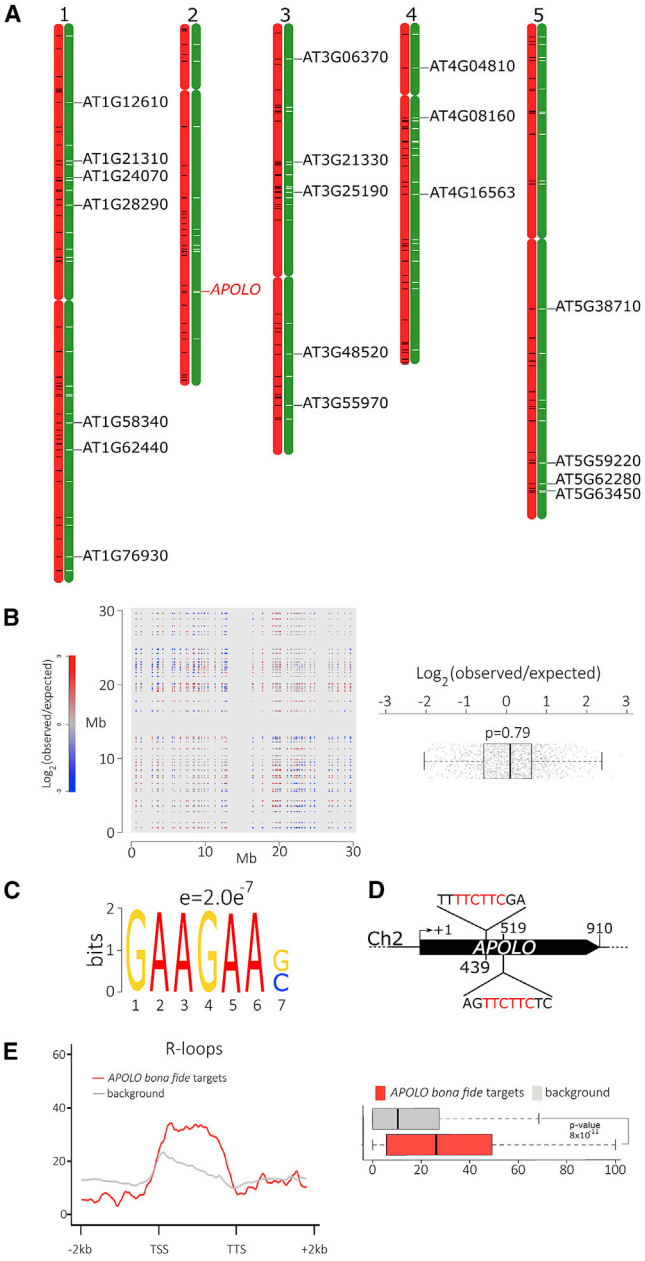

Figure 4. *APOLO* Multiple Independent Target Loci in *trans* Are Enriched in R-Loop Formation

(A) Genome-wide distribution of *APOLO bona fide* targets. In red chromosomes all 187 targets are shown as black lines. In green chromosomes, the 19 and 76 targets LHP1/*APOLO* targets (groups 2 and 3) are indicated as black lines. The 19 candidates in group 2 are indicated with the *Arabidopsis* identification code. *APOLO* is shown in red.

(B) Interaction plot of the *APOLO* targets located in chromosome 1. Chromatin-chromatin interactions among 20-kb bins bearing *APOLO* target loci are plotted. For each pair of these interactions, the observed/expected value was computed as the ratio of the observed HiC contact strength over all pairs of bins having the same genomic distance. The p value indicates the Mann-Whitney U test result.

(C) Consensus DNA motif in the peaks regions of *APOLO* targets, found by MEME-ChIP with default parameters (Bailey et al., 2009).

(D) Schematic representation of the *APOLO* locus, indicating the location of two TTCTTC cores encoding the UUCUUC transcript potentially matching the GAAGAA DNA cores forming R-loops.

(E) R-loop distribution pattern (tag density) over the gene body and flanking regions for all *Arabidopsis* genes (gray) and all 187 *APOLO bona fide* targets (red). TSS, transcription start site; TTS, transcription termination site. The metagene plot was generated using the R program. On the right, the same set of genes was used to calculate the percentage of overlapping between the gene body of each *APOLO* target and R-loop regions (red) and this was compared with the one obtained with the mean of all *Arabidopsis* genes (background). We found a statistically significant enrichment based on the p value of a Mann-Whitney U test.

See also Figures S4 and S5.

2015), to assess the direct binding of ARF7 over this region. In response to 15 min of exogenous IAA and dexamethasone induction, ARF7 was able to directly recognize one of the putative *cis*-acting elements, located at −2,974 bp upstream of the *APOLO* transcription start site (Figure S2C). Thus, our results indicate that *APOLO* is directly regulated by ARF7 and participates in the genetic regulatory network governing LR development.

To further decipher the role of *APOLO* in LR formation, we chose a subset of auxin-related genes (two from group 1, two from group 2, six from group 3, and one from group 4) to confirm *APOLO* binding to their genomic region by ChIRP-qPCR and its dependency on *APOLO* RNA (comparing WT versus *APOLO* RNAi plants; Figures 3E and S3A). Furthermore, we characterized for each locus the relative chromatin loop formation in WT versus *APOLO*-deregulated lines. All their chromatin loops were altered both by over-expression and knockdown of *APOLO*. In 7 out of the 11 cases analyzed, chromatin loop formation was enhanced in the RNAi plants and impaired in the *35S:APOLO* plants, respectively (Figures 3F and S3B). Accordingly, this set of genes was deregulated in the *35S:APOLO* (Figure 3G) and knockdown lines (Figures 2C and S3C). Furthermore, although *APOLO* RNAi plants previously did not show any evident LR phenotype (Ariel et al., 2014), *APOLO*-overexpressing lines exhibited an altered density of LRs in seedlings treated with auxin for one week (Figure 3H). Summing up, our data demonstrate that *APOLO* co-regulates auxin-responsive genes during LR development across the *Arabidopsis* genome.

Strikingly, the 187 *APOLO bona fide* targets were scattered across the *Arabidopsis* genome (Figure 4A), including the group 2 19 genes, which are *APOLO* and LHP1 targets, deregulated in the *35S:APOLO* and in the *lhp1* plants (Figure 1C, in the red circle). It was previously reported that chromatin-related lncRNAs modulate genes located in close spatial proximity within the nucleus (Simon et al., 2011; Maass et al., 2012; Engreitz et al., 2013; Hacisuleyman et al., 2014; Quinodoz and Guttman, 2014; Rinn and Guttman, 2014; West et al., 2014; Cloutier et al., 2016). Hence, using a previously published high-resolution HiC dataset (Liu et al., 2016) to search *APOLO* targets, we found that genomic regions bearing these 187 loci are apparently not spatially associated. Therefore, *APOLO* seemed to modulate non-associated local chromatin loops through a different mechanism than spatial proximity (Figure 4B; see Figure S4 for the full genome).

To further uncover the molecular mechanisms underlying *APOLO* recognition of distal independent targets, we looked

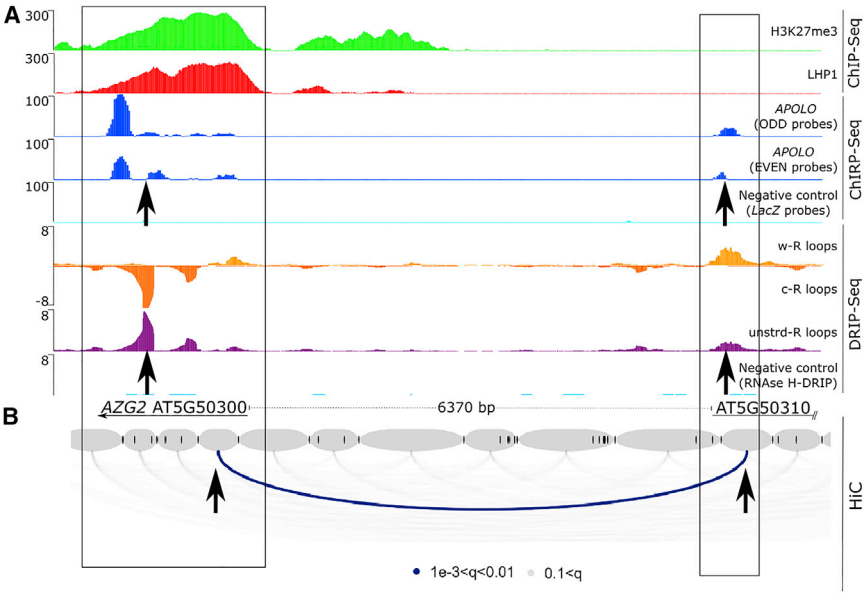

Figure 5. *APOLO* Recognition of Distal Targets Correlates with Genomic Regions Forming R-Loops

(A) Epigenomic landscape of the *AZG2* locus. Lane 1: H3K27me3 deposition by ChIP-seq (Veluchamy et al., 2016). Lane 2: LHP1 deposition by ChIP-seq (Veluchamy et al., 2016). Lanes 3–5: *APOLO* recognition by ChIRP-seq (lanes 3 and 4 positive, using ODD and EVEN sets of probes against *APOLO*, respectively; lane 5 negative control using LacZ probes). Lanes 6–9: R-loop formation by DRIP-seq (Xu et al., 2017), on Watson strand (lane 6), Crick strand (lane 7), or unstranded sequencing (lane 8). DRIP negative control after RNAseH treatment is shown in lane 9. Boxes indicate the regions over the two neighbor genes where *APOLO* binding correlates with R-loop formation. Gene annotations are shown below.

(B) Chromatin loops identified in the *AZG2* region by *Dpn*II HiC (Liu et al., 2016). Colors of the loops are related to the corresponding q values indicated below. Black arrows in (A) and (B) indicate the same genomic locations, where the bases of the chromatin loop correlate with R-loop formation and *APOLO* recognition. Gene annotations are shown above.

See also Data S1.

for any consensus motif enriched in the *APOLO* binding sites. Based on MEME-chromatin immunoprecipitation (ChIP) (Bailey et al., 2009), we determined a consensus sequence GAAGAA(G/C) (e value = 2.0 e^{-7}; Figure 4C). The extended consensus AGAAGAAGAA was also retrieved (e value = 2.2 e^{-91}; Figure S5A) among *APOLO* targets, in contrast to LacZ-ChIRP-seq (negative control; Figure S5B). Remarkably, this sequence coincides with the strand-specific consensus core recently reported for R-loops (Santos-Pereira and Aguilera, 2015) in *Arabidopsis*, determined by DRIP-seq (Xu et al., 2017). It is worth noting that *APOLO* exhibits two TTCTTC cores that could perfectly recognize the consensus motif in target genes by sequence complementarity (Figure 4D). Furthermore, the analysis of genome-wide identification of R-loops demonstrates that the 187 *APOLO bona fide* targets are significantly enriched in DNA-RNA duplexes (Figure 4E), suggesting that *APOLO* recognizes its target loci by sequence complementarity. For the two already validated targets, R-loops are detected at the 5′ region of the *PID* locus (Data S1A), and at the base of each side of the chromatin loop linking *WAG2* and At3g14400, where *APOLO* binds (Figure 2A; the DRIP-seq data lane is indicated with black arrows).

For further validation, we chose an additional auxin-responsive gene, *AZG2* (group 3), which was the most strongly affected *bona fide* target analyzed above, both at chromatin conformation level as well as transcriptional activity in *APOLO*-deregulated lines (Figures 3F, 3G, and S3). *AZG2* encodes a purine transporter and its transcriptional response to auxin is linked to LR initiation and development (Mansfield et al., 2009; Parizot, De Rybel and Beeckman, 2010). As shown in Figure 5A, *AZG2* exhibits H3K27me3 deposition, LHP1 enrichment, and *APOLO* RNA binding (by ChIRP-seq). Interestingly, R-loop presence (DRIP-seq data coverage) over the gene body correlates with the region of *APOLO* interaction deduced from ChIRP-seq coverage (the epigenetic landscapes of the other 10 loci validated in Figures 3E, 3F, and S3 are shown separately in Data S1B–S1J). According to our HiC dataset (Liu et al., 2016), a chromatin loop encompasses the 6.37-kb intergenic region between *AZG2* and the divergent upstream gene At5g50310, including the promoter of both genes (Figure 5B). Outstandingly, we can also detect *APOLO* binding and R-loop formation over the At5g50310 gene, thus at both sides of the chromatin loop (Figure 5A). As mentioned above, we validated the interaction of *APOLO* RNA with the *AZG2* locus and its dependency on *APOLO* by ChIRP-qPCR of WT versus *APOLO* RNAi plants (Figure 3E); we also determined by chromosome conformation capture (3C)-qPCR that chromatin loop formation was enhanced in the *APOLO* knockdown plants and impaired in the *35S:APOLO* plants (Figure 3F). Intergenic chromatin loop formation in these genotypes is in agreement with the transcriptional accumulation of the *AZG2* gene (Figures 3G and S3C). Furthermore, we validated by DRIP-qPCR the formation of an R-loop over the *AZG2* locus (Figure 6A), as well as over *PID* and *WAG2* (Figures S6A and S6D). The presence of the R-loops over *AZG2*, *PID*, and *WAG2* resulted in impairments in the RNAi *APOLO* lines, compared to the *APOLO*-independent R-loop over the sixth exon of the *SEP3* locus (Conn et al., 2017; Figures 6B, S6B, and S6E), supporting the role of *APOLO* in R-loop formation over target genes. Remarkably, using the antibody against DNA-RNA duplexes (monoclonal S6.9; Boguslawski et al., 1986; Chédin, 2016) for RNA immunoprecipitation (RIP) to detect RNAs present in these duplexes (alternatively called hereafter DRIP-RNA), we demonstrated that *APOLO* is present in *Arabidopsis* R-loops (Figure 6C). To further demonstrate the direct recognition of *APOLO* over target loci by R-loop formation, we developed a novel approach named RNA isolation by DNA

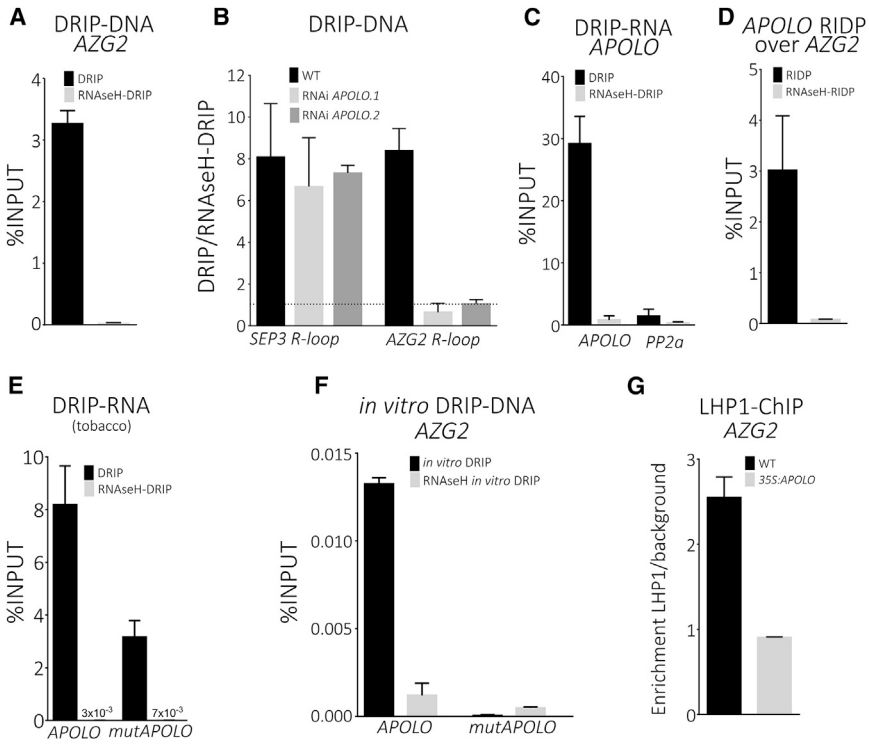

Figure 6. *APOLO* Recognition of Distal Targets Is Mediated by Sequence Complementarity and R-Loop Formation

(A) Validation of R-loop formation over the *AZG2* locus by DRIP-qPCR. RNAse H-treated samples are taken as the negative control.

(B) R-loop formation over the *AZG2* locus in WT vs two independent lines of RNAi *APOLO*. *SEP3* R-loop is independent of *APOLO* recognition and was taken as a negative control of R-loop decrease.

(C) *APOLO*-mediated R-loop formation was determined by RIP using the S9.6 antibody anti-R-loops (DRIP-RNA-qRT-PCR). The *APOLO* RNA is present when the IP is performed with anti-R-loop antibodies. *PP2a* mRNA was taken as a negative control.

(D) Validation of *APOLO*-mediated R-loop formation over the *AZG2* locus by RIDP-qPCR. Shortly, the *AZG2* DNA locus was purified using specific biotinylated probes, treated or not with RNAse H, and the associated RNA was isolated for qRT-PCR (see STAR Methods). RNAse H-treated samples are taken as the negative control, confirming that *APOLO* recognizes *AZG2* by DNA-RNA duplex formation.

(E) DRIP-RNA-qRT-PCR preformed using samples of *N. benthamiana* leaves transformed with *35S:APOLO* or *35S:mutAPOLO* (with both R-loop-related boxes mutagenized), showing that *APOLO* is more efficient in R-loop formation than *mutAPOLO*. In all biological replicates, the levels of *APOLO* and *mutAPOLO* were similar (16 < INPUT Ct < 17).

(F) Chromatin from *APOLO* RNAi plants was used for incubation with *in vitro*-transcribed *APOLO* or *mutAPOLO* and then a regular DRIP-qPCR over *AZG2* was performed. Only WT *APOLO* was able to restore R-loop formation over *AZG2*. Cts of input samples were equivalent between *APOLO* and *mutAPOLO* (between 17 and 18), indicating similar transcript stability.

(G) LHP1 deposition over the *AZG2* locus determined by ChIP-qPCR in WT and *35S:APOLO* plants. Overexpression of *APOLO* impairs recognition of the *AZG* target by LHP1. Error bars represent the SD of three biological replicates.

See also Figures S7 and S8 and Table S6.

purification (RIDP; Figure S7A). Briefly, we used biotinylated DNA probes to sequester specific loci from sonicated chromatin treated with T5 exonuclease, as previously used to purify chromatin-related proteins, (Murarka and Srivastava, 2018) (see STAR Methods). We specifically purified the loci of *AZG2*, *WAG2*, and *PID* DNAs and their associated RNAs using streptavidin-magnetic beads. As a control, we first checked the efficient purification of each DNA locus by RIDP-DNA-qPCR (Figure S7B). Then, we purified the RNAs associated to each locus by RIDP, treated or not with RNAseH, in order to specifically degrade RNAs forming R-loops. Finally, we determined by qRT-PCR whether the *APOLO* RNA was associated to each locus, in an R-loop dependent manner (Figures 6D, S7C, and S7D). Therefore, using two independent approaches (RIDP and R-loop antibodies for DRIP), we demonstrated that the *APOLO* RNA recognizes its distal target loci by establishing a DNA-RNA duplex.

To further assess the relevance of the two TTCTTC boxes in *APOLO* for R-loop formation, we generated an *APOLO* mutant version (*mutAPOLO*) with both boxes switched to AAGCTT (*Hind* III site) and GGATCC (*Bam*H I site), respectively. We used *Nicotiana benthamiana* as a heterologous system with no endogenous *APOLO* sequence to assess the capacity of the transgenes to form R-loops. Seventy-two hours after transient transformation of tobacco leaves, we purified nuclei and performed a DRIP-RNA assay. Strikingly, *mutAPOLO* was retrieved 60% less than its WT counterpart *APOLO*, indicating that the TTCTTC boxes are important for efficient R-loop formation *in planta* (Figure 6E). To further support the role of *APOLO* RNA in R-loop formation, we prepared chromatin extracts from *APOLO* RNAi plants (having impaired R-loop formation over *AZG2*, *WAG2*, and *PID*; Figures 6B, S6B, and S6E) to assess whether *in vitro*-transcribed *APOLO* or *mutAPOLO* were able to re-establish R-loop formation in these extracts. After 45 min of incubation of chromatin extracts with *in vitro*-transcribed RNA, we performed a DRIP-qPCR. Indeed, the ability of WT *APOLO* to restore R-loop formation over *AZG2* (Figure 6F), *WAG2*, and *PID* (Figures S6C and S6F) was successfully proven and this activity was abolished as a result of the mutations introduced in the *mutAPOLO* transcript. Thus, our findings demonstrate that the *APOLO* lncRNA specifically recognizes multiple distal DNA genomic regions by R-loop formation.

To explore how *APOLO* RNA controls chromatin loops in *trans*, we assessed whether LHP1 deposition on its targets is affected upon *APOLO* over-expression. Indeed, the 3D nuclear organization is strongly affected in *lhp1* mutants (Veluchamy et al., 2016), including the *PID-APOLO* chromatin loop (Ariel et al., 2014). To

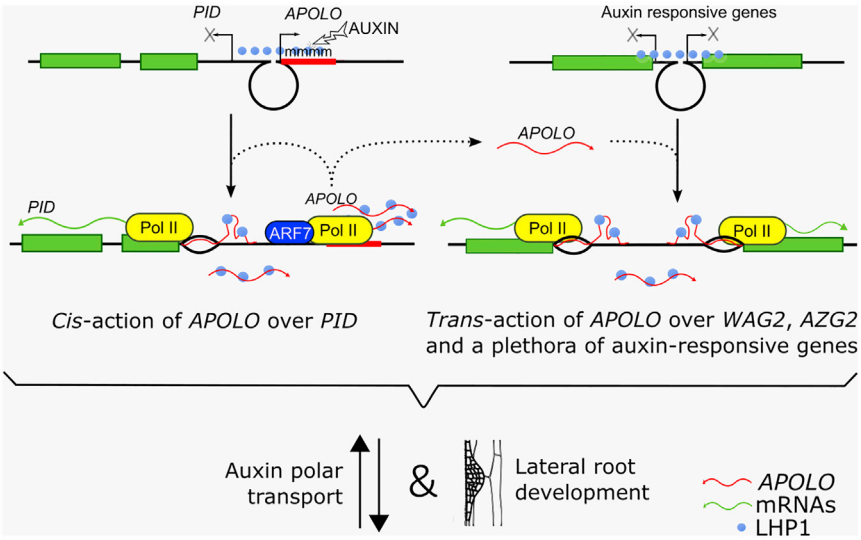

Figure 7. *trans*-Action of the *APOLO* Long Noncoding RNA Is Mediated by R-Loop Formation and Decoy of Polycomb Repressive Complex 1 Components

Model of *APOLO* regulation over multiple targets. In response to auxin, the *APOLO* locus is demethylated (Ariel et al., 2014) and the local chromatin loop is opened. *APOLO* and *PID* transcription is directly activated by ARF7. *APOLO* lncRNA binds to its neighboring locus *PID* forming an R-loop and decoying LHP1. *APOLO* also recognizes *WAG2*, *AZG2*, and multiple distant non-associated loci by R-loop formation. As a result, *APOLO* also decoys LHP1 modulating local chromatin loop formation. Alternatively, the transcriptional activation of *APOLO* targets by LHP1 decoy may trigger chromatin conformation changes. It remains unknown what additional components of the ribonucleic-protein complex are needed for the separation of DNA strands to allow R-loop formation. Altogether, our results indicate that *APOLO* co-regulates a plethora of auxin-responsive genes coordinating auxin distribution and lateral root formation.

this end, we performed ChIP-qPCR comparing WT versus *35S:APOLO* plants, showing that LHP1 recognition of the *AZG2* locus is reduced when *APOLO* is over-expressed (Figure 6G), as well as for *PID* and *WAG2* (Figure S8). Therefore, *APOLO* over-expression can impair LHP1 binding to distal targets, consequently impacting local 3D chromatin remodeling of multiple loci.

DISCUSSION

Altogether, our results indicate that *APOLO* directly controls its neighboring gene *PID* and a plethora of independent genes in *trans*. We propose that the interaction between *APOLO* and its targets is based on direct recognition by sequence complementarity and R-loop formation. *APOLO*-mediated R-loop formation does not occur by interaction of the nascent transcript with its own locus (Data S1A) further supporting that *APOLO* interacts with target DNA in *trans*, in addition to its neighboring locus, *PID*. The invasion of the DNA duplex by *APOLO* lncRNA results in the decoy of LHP1 and subsequent modulation of chromatin loop dynamics of its target loci. As a result, *APOLO* can coordinate transcription of topologically non-associated auxin-responsive genes during LR development by sequence-specific interaction and fine-tuning of local chromatin 3D conformation (Figure 7). Alternatively, it can be proposed that *APOLO*-mediated LHP1 decoy may trigger the transcription of the target loci, thus modulating local chromatin conformation. It is worth noting that the *APOLO* dynamic response to exogenous auxin previously reported (Ariel et al., 2014) is in agreement with the pattern of *APOLO* promoter activity shown here. The use of the reporter genes *GUS* and *GFP* indicates that *APOLO* is not accumulated in the LR apex, where a maximal concentration of auxin occurs (*DR5:RFP* signal) (Lavenus et al., 2013). At later stages of LR development, *APOLO* promoter remains active at the base of the LR (Figures 3B and 3C), in agreement with its relative decrease of transcriptional accumulation after 12 h of auxin treatment (Ariel et al., 2014). Here, we demonstrated that the *PID-APOLO* intergenic region is directly recognized by ARF7, a key regulator of LR development. Furthermore, the deregulation of *WAG2* in the RNAi *APOLO* plants in control conditions (Figure 2C) suggests that *APOLO* exerts an important role of transcriptional fine-tuning of *trans* targets in response to endogenous auxin.

In contrast to animals and other plant species, topologically associated domains (TADs) are hardly found in the *Arabidopsis thaliana* genome, which was attributed to the absence of homologs of canonical insulator proteins such as CTCF (Feng et al., 2014; Wang et al., 2015). However, high-resolution HiC approaches served to identify TAD-boundary-like and insulator-like regions (Wang et al., 2015), exhibiting similar properties to those of sequences at the borders of animal TADs. These findings hint at a strong connection between transcription and local chromatin topology (Lieberman-Aiden et al., 2009; Grob et al., 2014). The role of lncRNAs in genome topology modulation has been evidenced both in animals and plants (Ariel et al., 2014; Rinn and Guttman, 2014; Rodriguez-Granados et al., 2016). It was proposed that the nature of noncoding transcription *per se* can affect chromatin conformation in *cis*, although *trans* action was observed in cases where distal loci are brought into close spatial proximity within the cell nucleus (Rinn and Guttman, 2014). It was recently shown that the *Jpx* lncRNA expression from different genomic locations in transgenic mice can modulate *Xist* lncRNA activity in *trans* during chromosome X inactivation, although it remains uncertain how the endogenous *Jpx* lncRNA may control other topologically unrelated regions (Carmona et al., 2018). Also, it was recently proposed that the mouse *lincRNA-Cox2* can regulate its neighbor locus *Ptgs2* (coding for the prostaglandin-endoperoxide synthase) in *cis*, together with a subset of distant innate immune genes in *trans*, although the underlying mechanisms of the distal activity remain uncertain (Elling et al., 2018). Here, we uncovered how the *APOLO* lncRNA can recognize multiple distal loci belonging to spatially unrelated

compartments, although we cannot completely exclude that nuclear rearrangements in response to auxin may additionally bring *APOLO* targets into spatial proximity. Our results show that *APOLO* mediates the formation of R-loops by sequence complementarity with its targets, decoying PRC1 components and modulating local chromatin loop formation. We found that *APOLO* contains two TTCTTC boxes important for DNA-RNA duplex formation, complementary to the R-loop consensus GAAGAA core, highly represented throughout *APOLO bona fide* targets. Interestingly, two additional cores were retrieved by MEME-ChIP as significantly enriched among *APOLO* targets: CGGC(G/T) and CAAC(A/C)AC (Figure S7C). Based on BLAST, extended complementary regions were identified between *APOLO* and *PID*, and *WAG2* and *AZG2* (Figure S5D), respectively. Remarkably, the CGGC and CAAC cores were included in the extended complementary regions of *WAG2* and *AZG2*, respectively, suggesting that the *APOLO* TTCTTC cores are not the only boxes determining R-loop formation specificity, although they seem to be the main contributors to sequence complementarity according to our results. Recently, two evolutionary related proteins called ALBA 1 and 2 were identified in *Arabidopsis* as R-loop readers involved in genome stability (Yuan et al., 2019). Further work will be needed to identify protein complexes participating in R-loop formation as well as the determination of lncRNA-*trans* target specificity.

The identification of genome-wide formation of R-loops in *Arabidopsis* revealed that DNA-RNA duplexes are strongly enriched in gene promoters and gene bodies (Xu et al., 2017). Interestingly, the deposition of the repressive mark H3K27me3 shows a global anti-correlation with R-loop presence over gene bodies. However, we have found a subset of genes showing an enriched deposition of H3K27me3, LHP1 recognition, and *APOLO*-mediated R-loop formation. Although R-loops are common features in the *Arabidopsis* genome (Xu et al., 2017), our findings suggest that their singularities in the context of chromatin compaction and function may be partially linked to the role of lncRNAs in genome organization and gene transcriptional regulation. It was recently shown in HeLa cells that the depletion of the Pol-II-associated transcription elongation factor SPT6 affects the distribution of H3K36me3 histone marks promoting the transcription of extended, polyadenylated lncRNAs prone to form local R-loops associated with DNA damage (Nojima et al., 2018). These findings suggest that the epigenomic context restricts noncoding transcription and excessive R-loop formation in *cis* to warrantee genome integrity and avoid transcription-replication collision.

Remarkably, the sequence consensus of human R-loops consists of a polypurine (GGAA)n core (Nadel et al., 2015), similar to the purine-rich GAAGAA motif reported in *Arabidopsis* (Xu et al., 2017). Furthermore, R-loop formation positively correlates with H3K27me3 deposition in humans (Nadel et al., 2015), resembling *APOLO*-targeted loci, mediated by DNA-RNA interaction. Also, R-loops correlate with low DNA methylated regions both in animals and plants, hinting at further commonalities (Ginno et al., 2012; Xu et al., 2017). Altogether, common R-loops characteristics between *Arabidopsis* and humans highlight that formation of DNA-RNA duplexes may be a conserved mechanism for target recognition and *trans* action of lncRNAs across kingdoms. Moreover, PRC1 components can bind to lncRNAs in animals and it was proposed, among other hypotheses, that this interaction could guide the ribonucleoprotein complex to specific gene loci (Ray et al., 2016). Like plant LHP1, animal chromodomain-containing proteins were shown to recognize lncRNAs *in vivo* (Piacentini et al., 2009; Yap et al., 2010). Our results suggest that PRC1 components and chromodomain-containing proteins can be specifically decoyed from chromatin targets by R-loop-related lncRNAs. In addition, considering that the short R-loop consensus motif hinders an easy prediction of other *APOLO*-like *trans*-acting lncRNAs, DRIP-RNA-seq (or S9.6 antibody RIP-seq) in different model organisms will be of key importance for genome-wide identification of R-loop-associated lncRNAs. Previously, two characterized R-loops in *Arabidopsis* uncovered the action in *cis* of noncoding transcripts, involved in transcriptional self-repression or alternative splicing, respectively (Sun et al., 2013; Conn et al., 2017). Our findings challenge the concept of a distance-based restriction for lncRNA action, expanding the possibilities about how noncoding transcripts shape genome three-dimensional organization and coordinate the activity of distal unrelated loci.

STAR★METHODS

Detailed methods are provided in the online version of this paper and include the following:

- KEY RESOURCES TABLE
- LEAD CONTACT AND MATERIALS AVAILABILITY
- EXPERIMENTAL MODEL AND SUBJECT DETAILS
- METHOD DETAILS
  - RT-qPCR
  - Chromatin Immunoprecipitation Assay
  - Chromatin Isolation by RNA Purification Assay
  - Chromosome Conformation Capture Assay (3C)
  - DNA-RNA duplex Immunopurification assay (DRIP-DNA-qPCR and DRIP-RNA-RT-qPCR)
  - In vitro DNA-RNA duplex Immunopurification assay (in vitro DRIP-DNA-qPCR)
  - RNA Isolation by DNA Purification (RIDP)
  - GUS Staining and GFP Confocal Microcopy
- QUANTIFICATION AND STATISTICAL ANALYSIS
- DATA AND CODE AVAILABILITY

SUPPLEMENTAL INFORMATION

Supplemental Information can be found online at https://doi.org/10.1016/j.molcel.2019.12.015.

A video abstract is available at https://doi.org/10.1016/j.molcel.2019.12.015#mmc9.

ACKNOWLEDGMENTS

We want to thank Dr. Tom Beeckman for the seeds of Pro_{ARF7}:*ARF7-GR* transformed plants. This work was supported by grants from ANPCyT (PICT 2016-0289 and 2016-0007, Agencia Nacional de Promoción Científica y Tecnológica, Argentina); CNRS (Laboratoire International Associé NOCOSYM); the Laboratoire d'Excellence (LABEX) Saclay Plant Sciences (SPS; ANR-10-LABX-40); and ANR grants (ANR 15-CE20-0002-01 EPISYM

and ANR 16-CE20-0003-04 SPLISIL), as well as the EPIMMUNITY International project between IPS2, France, and KAUST University, Saudi Arabia.

AUTHOR CONTRIBUTIONS

F.A., M.C., and M.B. designed the research. F.A., A.C., L.L., M.F.M., and T.J. performed the experiments. D.L., T.B., K.M., A.V., and C.L. analyzed the data. F.A. and M.C. wrote the manuscript. All authors revised and discussed the manuscript.

DECLARATION OF INTERESTS

The authors declare no competing interests.

Received: April 25, 2019
Revised: August 30, 2019
Accepted: December 18, 2019
Published: January 14, 2020

REFERENCES

Ariel, F., Jegu, T., Latrasse, D., Romero-Barrios, N., Christ, A., Benhamed, M., and Crespi, M. (2014). Noncoding transcription by alternative RNA polymerases dynamically regulates an auxin-driven chromatin loop. Mol. Cell *55*, 383–396.

Armengot, L., Marquès-Bueno, M.M., and Jaillais, Y. (2016). Regulation of polar auxin transport by protein and lipid kinases. J. Exp. Bot. *67*, 4015–4037.

Bailey, T.L., Boden, M., Buske, F.A., Frith, M., Grant, C.E., Clementi, L., Ren, J., Li, W.W., and Noble, W.S. (2009). MEME SUITE: tools for motif discovery and searching. Nucleic Acids Res. *37* (*Suppl. 2*), W202–W208.

Bazin, J., Romero, N., Rigo, R., Charon, C., Blein, T., Ariel, F., and Crespi, M. (2018). Nuclear Speckle RNA Binding Proteins Remodel Alternative Splicing and the Non-coding Arabidopsis Transcriptome to Regulate a Cross-Talk Between Auxin and Immune Responses. Front. Plant Sci. *9*, 1208.

Berry, S., Rosa, S., Howard, M., Bühler, M., Dean, and C. (2017). Disruption of an RNA-binding hinge region abolishes LHP1- mediated epigenetic repression. Genes Dev. *31*, 2115–2120.

Boguslawski, S.J., Smith, D.E., Michalak, M.A., Mickelson, K.E., Yehle, C.O., Patterson, W.L., and Carrico, R.J. (1986). Characterization of monoclonal antibody to DNA.RNA and its application to immunodetection of hybrids. J. Immunol. Methods *89*, 123–130.

Carmona, S., Lin, B., Chou, T., Arroyo, K., and Sun, S. (2018). LncRNA Jpx induces Xist expression in mice using both trans and cis mechanisms. PLoS Genet. *14*, e1007378.

Chédin, F. (2016). Nascent Connections: R-Loops and Chromatin Patterning. Trends Gen. *32*, 828–838.

Cloutier, S.C., Wang, S., Ma, W.K., Al Husini, N., Dhoondia, Z., Ansari, A., Pascuzzi, P.E., and Tran, E.J. (2016). Regulated Formation of lncRNA-DNA Hybrids Enables Faster Transcriptional Induction and Environmental Adaptation. Mol. Cell *61*, 393–404.

Conn, V.M., Hugouvieux, V., Nayak, A., Conos, S.A., Capovilla, G., Cildir, G., Jourdain, A., Tergaonkar, V., Schmid, M., Zubieta, C., and Conn, S.J. (2017). A circRNA from SEPALLATA3 regulates splicing of its cognate mRNA through R-loop formation. Nat. Plants *3*, 17053.

Czechowski, T., Stitt, M., Altmann, T., Udvardi, M.K., and Scheible, W.-R. (2005). Genome-Wide Identification and Testing of Superior Reference Genes for Transcript Normalization. Plant Physiol. *139*, 5–17.

Dhonukshe, P., Huang, F., Galvan-Ampudia, C.S., Mähönen, A.P., Kleine-Vehn, J., Xu, J., Quint, A., Prasad, K., Friml, J., Scheres, B., and Offringa, R. (2015). Plasma membrane-bound AGC3 kinases phosphorylate PIN auxin carriers at TPRXS(N/S) motifs to direct apical PIN recycling. Development *142*, 2386–2387.

Elling, R., Robinson, E.K., Shapleigh, B., Liapis, S.C., Covarrubias, S., Katzman, S., Groff, A.F., Jiang, Z., Agarwal, S., et al. (2018). Genetic Models Reveal *cis* and *trans* Immune-Regulatory Activities for lincRNA-Cox2. Cell Rep. *25*, 1511–1524.e6.

Engreitz, J.M., Pandya-Jones, A., McDonel, P., Shishkin, A., Sirokman, K., Surka, C., Kadri, S., Xing, J., Goren, A., Lander, E.S., et al. (2013). The Xist lncRNA exploits three-dimensional genome architecture to spread across the X chromosome. Science *341*, 1237973.

Feng, S., Cokus, S.J., Schubert, V., Zhai, J., Pellegrini, M., and Jacobsen, S.E. (2014). Genome-wide Hi-C analyses in wild-type and mutants reveal high-resolution chromatin interactions in Arabidopsis. Mol. Cell *55*, 694–707.

Ginno, P.A., Lott, P.L., Christensen, H.C., Korf, I., and Chédin, F. (2012). R-Loop Formation Is a Distinctive Characteristic of Unmethylated Human CpG Island Promoters. Mol. Cell *45*, 814–825.

Grob, S., Schmid, M.W., and Grossniklaus, U. (2014). Hi-C Analysis in Arabidopsis Identifies the KNOT, a Structure with Similarities to the flamenco Locus of Drosophila. Mol. Cell *55*, 678–693.

Hacisuleyman, E., Goff, L.A., Trapnell, C., Williams, A., Henao-Mejia, J., Sun, L., McClanahan, P., Hendrickson, D.G., Sauvageau, M., Kelley, D.R., et al. (2014). Topological organization of multichromosomal regions by the long intergenic noncoding RNA Firre. Nat. Struct. Mol. Biol. *21*, 198–206.

Heinz, S., Benner, C., Spann, N., Bertolino, E., Lin, Y.C., Laslo, P., Cheng, J.X., Murre, C., Singh, H., and Glass, C.K. (2010). Simple combinations of lineage-determining transcription factors prime cis-regulatory elements required for macrophage and B cell identities. Mol. Cell *38*, 576–589.

Himanen, K., Boucheron, E., Vanneste, S., de Almeida Engler, J., Inzé, D., and Beeckman, T. (2002). Auxin-Mediated Cell Cycle Activation during Early Lateral Root Initiation. Plant Cell *14*, 2339–2351.

Jégu, T., Aeby, E., and Lee, J.T. (2017). The X chromosome in space. Nat. Rev. Genet. *18*, 377–389.

Langmead, B., and Salzberg, S.L. (2012). Fast gapped-read alignment with Bowtie 2. Nat. Methods *9*, 357–360.

Lavenus, J., Goh, T., Roberts, I., Guyomarc'h, S., Lucas, M., De Smet, I., Fukaki, H., Beeckman, T., Bennett, M., and Laplaze, L. (2013). Lateral root development in Arabidopsis: fifty shades of auxin. Trends Plant Sci. *18*, 450–458.

Lavenus, J., Goh, T., Guyomarc'h, S., Hill, K., Lucas, M., Voß, U., Kenobi, K., Wilson, M.H., Farcot, E., Hagen, G., et al. (2015). Inference of the Arabidopsis lateral root gene regulatory network suggests a bifurcation mechanism that defines primordia flanking and central zones. Plant Cell *27*, 1368–1388.

Lewis, D.R., Olex, A.L., Lundy, S.R., Turkett, W.H., Fetrow, J.S., and Muday, G.K. (2013). A kinetic analysis of the auxin transcriptome reveals cell wall remodeling proteins that modulate lateral root development in Arabidopsis. Plant Cell *25*, 3329–3346.

Lieberman-Aiden, E., van Berkum, N.L., Williams, L., Imakaev, M., Ragoczy, T., Telling, A., Amit, I., Lajoie, B.R., Sabo, P.J., Dorschner, M.O., et al. (2009). Comprehensive mapping of long-range interactions reveals folding principles of the human genome. Science *326*, 289–293.

Liu, C., Wang, C., Wang, G., Becker, C., Zaidem, M., and Weigel, D. (2016). Genome-wide analysis of chromatin packing in Arabidopsis thaliana at single-gene resolution. Genome Res. *26*, 1057–1068.

Maass, P.G., Rump, A., Schulz, H., Stricker, S., Schulze, L., Platzer, K., Aydin, A., Tinschert, S., Goldring, M.B., Luft, F.C., and Bähring, S. (2012). A misplaced lncRNA causes brachydactyly in humans. J. Clin. Invest. *122*, 3990–4002.

Malamy, J.E., and Benfey, P.N. (1997). Organization and cell differentiation in lateral roots of Arabidopsis thaliana. Development *124*, 33–44.

Manavella, P.A., Dezar, C.A., Ariel, F.D., and Chan, R.L. (2008). Two ABREs, two redundant root-specific and one W-box cis-acting elements are functional in the sunflower HAHB4 promoter. Plant Physiol, Biochem. *46*, 860–867.

Mansfield, T.A., Schultes, N.P., and Mourad, G.S. (2009). AtAzg1 and AtAzg2 comprise a novel family of purine transporters in Arabidopsis. FEBS Lett. *583*, 481–486.

Marin, E., Jouannet, V., Herz, A., Lokerse, A.S., Weijers, D., Vaucheret, H., Nussaume, L., Crespi, M.D., and Maizel, A. (2010). miR390, Arabidopsis TAS3 tasiRNAs, and their AUXIN RESPONSE FACTOR targets define an

autoregulatory network quantitatively regulating lateral root growth. Plant Cell *22*, 1104–1117.

Moreno, A.B., Martínez de Alba, A.E., Bardou, F., Crespi, M.D., Vaucheret, H., Maizel, A., and Mallory, A.C. (2013). Cytoplasmic and nuclear quality control and turnover of single-stranded RNA modulate post-transcriptional gene silencing in plants. Nucleic Acids Res. *41*, 4699–4708.

Murarka, P., and Srivastava, P. (2018). An improved method for the isolation and identification of unknown proteins that bind to known DNA sequences by affinity capture and mass spectrometry. PLoS One *13*, e0202602.

Musielak, T.J., Schenkel, L., Kolb, M., Henschen, A., and Bayer, M. (2015). A simple and versatile cell wall staining protocol to study plant reproduction. Plant Reprod. *28*, 161–169.

Nadel, J., Athanasiadou, R., Lemetre, C., Wijetunga, N.A., Ó Broin, P., Sato, H., Zhang, Z., Jeddeloh, J., Montagna, C., Golden, A., et al. (2015). RNA:DNA hybrids in the human genome have distinctive nucleotide characteristics, chromatin composition, and transcriptional relationships. Epigenetics Chromatin. *8*, 46.

Nojima, T., et al. (2018). Deregulated Expression of Mammalian lncRNA through Loss of SPT6 Induces R-Loop Formation, Replication Stress, and Cellular Senescence. Mol. Cell *72*, 970–984.e7.

Parizot, B., De Rybel, B., and Beeckman, T. (2010). VisuaLRTC: a new view on lateral root initiation by combining specific transcriptome data sets. Plant Physiol. *153*, 34–40.

Piacentini, L., Fanti, L., Negri, R., Del Vescovo, V., Fatica, A., Altieri, F., and Pimpinelli, S. (2009). Heterochromatin protein 1 (HP1a) positively regulates euchromatic gene expression through RNA transcript association and interaction with hnRNPs in Drosophila. PLoS Genet. *5*, e1000670.

Quinodoz, S., and Guttman, M. (2014). Long noncoding RNAs: an emerging link between gene regulation and nuclear organization. Trends Cell Biol. *24*, 651–663.

Ray, M.K., Wiskow, O., King, M.J., Ismail, N., Ergun, A., Wang, Y., Plys, A.J., Davis, C.P., Kathrein, K., Sadreyev, R., et al. (2016). CAT7 and cat7l long non-coding rnas tune polycomb repressive complex 1 function during human and zebrafish development. J. Biol. Chem. *291*, 19558–19572.

Rinn, J., and Guttman, M. (2014). RNA Function. RNA and dynamic nuclear organization. Science *345*, 1240–1241.

Rodriguez-Granados, N.Y., Ramirez-Prado, J.S., Veluchamy, A., Latrasse, D., Raynaud, C., Crespi, M., Ariel, F., and Benhamed, M. (2016). Put your 3D glasses on: plant chromatin is on show. J. Exp. Bot. *67*, 3205–3221.

Santos-Pereira, J.M., and Aguilera, A. (2015). R loops: new modulators of genome dynamics and function. Nat. Rev. Genet. *16*, 583–597.

Seo, J.S., Sun, H.X., Park, B.S., Huang, C.H., Yeh, S.D., Jung, C., and Chua, N.H. (2017). ELF18-INDUCED LONG-NONCODING RNA Associates with Mediator to Enhance Expression of Innate Immune Response Genes in Arabidopsis. Plant Cell *29*, 1024–1038.

Shen, L., Shao, N., Liu, X., and Nestler, E. (2014). ngs.plot: Quick mining and visualization of next-generation sequencing data by integrating genomic databases. BMC Genomics *15*, 284.

Simon, M.D., Wang, C.I., Kharchenko, P.V., West, J.A., Chapman, B.A., Alekseyenko, A.A., Borowsky, M.L., Kuroda, M.I., and Kingston, R.E. (2011). The genomic binding sites of a noncoding RNA. Proc. Natl. Acad. Sci. USA *108*, 20497–20502.

Sun, Q., Csorba, T., Skourti-Stathaki, K., Proudfoot, N.J., and Dean, C. (2013). R-loop stabilization represses antisense transcription at the Arabidopsis FLC locus. Science *340*, 619–621.

Trapnell, C., Pachter, L., and Salzberg, S.L. (2009). TopHat: discovering splice junctions with RNA-Seq. Bioinformatics *25*, 1105–1111.

Trapnell, C., Williams, B.A., Pertea, G., Mortazavi, A., Kwan, G., van Baren, M.J., Salzberg, S.L., Wold, B.J., and Pachter, L. (2010). Transcript assembly and quantification by RNA-Seq reveals unannotated transcripts and isoform switching during cell differentiation. Nat. Biotechnol. *28*, 511–515.

Turck, F., Roudier, F., Farrona, S., Martin-Magniette, M.L., Guillaume, E., Buisine, N., Gagnot, S., Martienssen, R.A., Coupland, G., and Colot, V. (2007). Arabidopsis TFL2/LHP1 specifically associates with genes marked by trimethylation of histone H3 lysine 27. PLoS Genet. *3*, e86.

Veluchamy, A., Jégu, T., Ariel, F., Latrasse, D., Mariappan, K.G., Kim, S.K., Crespi, M., Hirt, H., Bergounioux, C., Raynaud, C., and Benhamed, M. (2016). LHP1 Regulates H3K27me3 Spreading and Shapes the Three-Dimensional Conformation of the Arabidopsis Genome. PLoS ONE *11*, e0158936.

Wang, C., Liu, C., Roqueiro, D., Grimm, D., Schwab, R., Becker, C., Lanz, C., and Weigel, D. (2015). Genome-wide analysis of local chromatin packing in Arabidopsis thaliana. Genome Res. *25*, 246–256.

West, J.A., Davis, C.P., Sunwoo, H., Simon, M.D., Sadreyev, R.I., Wang, P.I., Tolstorukov, M.Y., and Kingston, R.E. (2014). The long noncoding RNAs NEAT1 and MALAT1 bind active chromatin sites. Mol. Cell *55*, 791–802.

Xu, W., Xu, H., Li, K., Fan, Y., Liu, Y., Yang, X., and Sun, Q. (2017). The R-loop is a common chromatin feature of the Arabidopsis genome. Nat. Plants *3*, 704–714.

Yap, K.L., Li, S., Muñoz-Cabello, A.M., Raguz, S., Zeng, L., Mujtaba, S., Gil, J., Walsh, M.J., and Zhou, M.M. (2010). Molecular interplay of the noncoding RNA ANRIL and methylated histone H3 lysine 27 by polycomb CBX7 in transcriptional silencing of INK4a. Mol. Cell *38*, 662–674.

Yuan, W., Zhou, J., Tong, J., Zhuo, W., Wang, L., Li, Y., Sun, Q., and Qian, W. (2019). ALBA protein complex reads genic R-loops to maintain genome stability in Arabidopsis. Sci. Adv. *5*, eaav9040.

Zhang, Y., Liu, T., Meyer, C.A., Eeckhoute, J., Johnson, D.S., Bernstein, B.E., Nusbaum, C., Myers, R.M., Brown, M., Li, W., and Liu, X.S. (2008). Model-based Analysis of ChIP-Seq (MACS). Genome Biol. *9*, R137.

STAR★METHODS

KEY RESOURCES TABLE

REAGENT or RESOURCE	SOURCE	IDENTIFIER
Antibodies		
Anti-LHP1	Covalab	pab0923-P
Anti-GF	Abcam	ab3580
Anti-IgG	Abcam	Ab6702
Anti-R-loop (S9.6)	Millipore	MABE1095
Deposited Data		
ChiRP-Seq and RNA-Seq	NCBI-GEO	GSE117486
H3K27me3 ChIP-Seq	NCBI-GEO	GSE76571
LHP1 ChIP-Seq	NCBI-GEO	GSE76571
DRIP-Seq	NCBI-GEO	GSE95765
HiC	NCBI-SRA	SRP064711
Imaging raw data	Mendeley Data	https://dx.doi.org/10.17632/z4j5zn2wc7.1
Experimental Models: Organisms		
Arabidopsis thaliana Col0	N/A	N/A
A. thaliana APOLO RNAi (2 lines)	Ariel et al., 2014	*APOLO* RNAi 1&2
A. thaliana 35:S:APOLO (2 lines)	This paper	*35S:APOLO* 1&2
A. thaliana arf7/19, proARF7:ARF7:GR	Lavenus et al., 2015	PRO_{ARF7}*:ARF7-GR*
A. thaliana ProAPOLO:GFP:GUSxDR5	This paper	*ProAPOLO:GFPxDR5*
Oligonucleotides		
ChIRP-Seq biotinylated probes	Ariel et al., 2014	ODD, EVEN and Lacz sets
RT-qPCR	This paper	Table S4
DRIP/ChIRP	This paper	Table S4
RIDP	This paper	Table S4
3C	This paper	Table S4
Cloning	This paper	Table S4
Software and Algorithms		
TopHat v2.0.9	Trapnell et al., 2009	N/A
Cufflinks v2.2.0	Trapnell et al., 2010	N/A
Bowtie	Langmead and Salzberg, 2012	N/A
MACS2	Zhang et al., 2008	N/A
HOMER	Heinz et al., 2010	N/A
NGSplot	Shen et al., 2014	N/A

LEAD CONTACT AND MATERIALS AVAILABILITY

Further information and requests for resources and reagents should be directed to and will be fulfilled by the Lead Contact, Federico Ariel (fariel@santafe-conicet.gov.ar)

Plant lines generated in this study are available from the Lead Contact with a completed Materials Transfer Agreement.

EXPERIMENTAL MODEL AND SUBJECT DETAILS

All lines used are in Columbia-0 background. Plants were grown in long day (16 h light, 90 $\mu E\ m^{-2}\ sec^{-1}$/8 h dark) at 23 °C on solid half-strength MS medium (MS/2, Duchefa). *E. coli* DH5a was used for subcloning, and *Agrobacterium tumefaciens* Agl-0 was used for plant transformation. The RNAi lines were previously reported (Ariel et al., 2014). The *APOLO* over expressing lines were obtained by transforming Col-0 plants using the full-length *APOLO* region under the control of the 35S promoter in the vector pB7WG2.

For the auxin treatment for RNA extraction, 1-week-old seedlings grown in MS/2 (on nylon membranes) were transferred to plates containing MS/2 + 10 μM 1-N-Naphthylphthalamic acid (NPA), an inhibitor of auxin transport (Himanen et al., 2002). After 3 days, seedlings were transferred to MS/2 plates containing synthetic auxin 10 μM 1-Naphthaleneacetic acid (NAA). Samples were taken at 12hr of treatment, after crosslinking or not, depending on the experiment. Total RNA samples for RNA-seq of three biological replicates for each genotype were prepared with the ZR Plant RNA MiniPrep kit (Zymo Research), according to the manufacturer's instructions. Libraries were prepared for Illumina and sequenced by Zymo Research (oriented 75bp long single ends). For phenotypic characterization of root development, plants were directly germinated in 0.1 μM NAA. Pictures were taken at 7 days and measured using the ImageJ software.

METHOD DETAILS

RT-qPCR

Total RNA was prepared using TRI Reagent (Sigma-Aldrich) and treated with DNase (Fermentas). A total of 1 μg of RNA was used for oligo(dT) reverse transcription (SuperScriptII, Invitrogen). RT-qPCR primers are available in Table S4. RT-qPCR was performed using a Roche Light Cycler 480 standard protocol (40 cycles, 60°C annealing) and analyzed using the delta delta Ct method using two constitutive genes (AT1G13320 and AT4G26410 (Czechowski et al., 2005)).

Chromatin Immunoprecipitation Assay

Chromatin immunoprecipitation (ChIP) assays were performed on 10-day-old seedlings using anti-LHP1 (Covalab pab0923-P) and anti-IgG (Abcam ab6702), as previously described (Ariel et al., 2014). Briefly, 1% formaldehyde-crosslinked chromatin was extracted by cell resuspension (10mM Tris-HCl pH8, 0,4M sucrose, 10mM $MgCl_2$, 5mM βME, RNAse.In SIGMA R7397), centrifugation, cell membrane lysis (10mM Tris-HCl pH8, 0,25M sucrose, 10mM $MgCl_2$, 5mM βME, 1% TRITON X100, 200 μM PMSF), and sucrose gradient formed by a lower layer of pure buffer (10mM Tris-HCl pH8, 1.7M sucrose, 2mM $MgCl_2$, 5mM βME, 0.15% TRITON X100) and an upper layer of resuspended pellet in the same buffer. Nuclei were resuspended in 300 μl of Nuclei Lysis Buffer (50mM Tris-HCl pH8, 0.1% SDS, 10mM EDTA, 1 μl of 20U/μl RNAase-in Promega per sample) and was sonicated using a water bath Bioruptor Pico (Diagenode; 30 s on/ 30 s off pulses, at high intensity for 10 cycles). ChIP was performed using Invitrogen Protein A Dynabeads. Immunoprecipitated DNA was recovered using Phenol:Chloroform:Isoamilic Acid (25:24:1; Sigma) and analyzed by qPCR. Untreated sonicated chromatin was processed in parallel and considered the Input sample.

For ARF7-GR ChIP qPCR over the *PID-APOLO* intergenic region, transgenic *arf7 arf19* double mutant plants complemented by expressing a dexamethasone (DEX) inducible ARF7-GLUTICORTICOID RECEPTOR (GR) fusion protein under the native ARF7 promoter were used (Lavenus et al., 2015). Plants were grown in Petri dishes under control conditions for 11 days and then treated with 1 μM IAA and 2 μM DEX for 15 min. For ChIP, an anti-GR antibody was used (Abcam ab3580), together with the anti-IgG previously described as a negative control for immunoprecipitation assays.

Chromatin Isolation by RNA Purification Assay

Chromatin isolation by RNA purification (ChIRP) was performed basically as described previously, using the same sets of antisense biotynilated DNA probes (Ariel et al., 2014). For ChIRP-Seq, 9g of seedlings crosslinked by UV exposure. The crosslinked seedlings were ground and nuclei were isolated (as for ChIP) and sonicated using a water bath Bioruptor Plus (Diagenode; 30 s on/ 30 s off pulses, at high intensity for 30 cycles). Chromatin was diluted in 2 volume of hybridization buffer (750 mM NaCl, 1% SDS, 50 mM Tris 7.0, 1 mM EDTA, 15% formamide, add DTT, PMSF, Protease Inhibitor (Sigma-Aldrich) and Superase-in (Ambion). Probes of 100 pmol were added to 200 μl of diluted chromatin, which was incubated at 50 °C for 4 hr. Streptavidin- magnetic C1 beads (Invitrogen) were washed three times in nuclear hybridization buffer. Fifty microliters of washed beads were added, and the whole reaction (beads:biotin-probes:RNA:chromatin) was incubated 60 min at 50°C. After incubation, beads were washed four times with 100 μl of ChIRP wash buffer (2X SSC, 0.5% SDS, add DTT and PMSF fresh). After last wash, beads were deposed in elution buffer (50 mM NaHCO3, 1% SDS, 200 mM NaCl), and DNA was eluted with a cocktail of 100 μg/ml RNase A (Sigma-Aldrich) and 0.1 U/ml RNase H (Ambion). Reverse crosslinking was performed with Proteinase K, for 1 hr at 65 °C. The obtained DNA was recovered using Phenol:Chloroform:Isoamyl Acid (25:24:1; Sigma) and used for library construction. Three independent libraries were prepared using the NEBNext Ultra DNA Library Prep Kit for Illumina, for ODD, EVEN and LacZ probes-derived samples, respectively. An additional ODD biological replicate was sequenced. As indicated in Table S1, 99% of the potential targets (8861/8941) identified in the first ODD sample were confirmed in the second sample, as well as 186 out of the 187 *APOLO bona fide* targets (Table S1, bottom right panel). The first ODD sample was used for further analyses given the higher library homogeneity across samples with EVEN and LacZ (See Table S5).

Chromosome Conformation Capture Assay (3C)

Chromosome conformation capture (3C) was performed basically as previously described (Ariel et al., 2014) starting with two grams of seedlings. Digestions were performed overnight at 37°C with 400 U DpnII (NEB). DNA was ligated by incubation in a shaker at 16°C, 100 rpm, for 5 h in 4 ml volume using 100U of T4 DNA ligase (NEB). After reverse crosslinking and Proteinase K treatment (Invitrogen),

DNA was recovered by Phenol:Chloroform:Isoamyl Acid (25:24:1; Sigma) extraction and ethanol precipitation. Relative interaction frequency was calculated by qPCR. A region free of DpnII was used to normalize the amount of DNA.

DNA-RNA duplex Immunopurification assay (DRIP-DNA-qPCR and DRIP-RNA-RT-qPCR)

For DNA-RNA duplex immunopurification, non-crosslinked seedlings were used for nuclei purification and samples were sonicated as for ChIP. Chromatin samples were incubated with 50 μl of washed Protein G Dynabeads pre-coated with 1μg of S9.6 antibody (Millipore MABE1095) for 16 h at 4 °C. RNAseH (Invitrogen)-treated samples for 2h at 37 °C were used for DRIP in parallel as a negative control. After washing, DNA was recovered for qPCR over R-loop related loci. Alternatively, RNA was recovered using RNAZol (MRC) and used for RT using random hexamers and *APOLO* qPCR, using *PP2a* mRNA as a negative control. For the validation of the R-loop related boxes in *APOLO*, *Nicotiana benthamiana* leaves were transformed as previously described (Moreno et al., 2013) using the *35S:APOLO* or the *35S:mutAPOLO* constructs (synthesized by Genewizz), recombined into a plasmid p35S-GW-6xMS2 (Seo et al., 2017), and after 72h samples were harvested and the DRIP-RNA-RT-qPCR was performed as described above. Washes of DRIP samples were performed using ChIRP Washing Buffer. The full sequence of *APOLO* and *mutAPOLO* are available in Table S6.

In vitro DNA-RNA duplex Immunopurification assay (in vitro DRIP-DNA-qPCR)

APOLO and *mutAPOLO* plasmids were used for *APOLO* DNA amplification including the T7 promoter on the 5' PCR primer. PCR products were checked by agarose electrophoresis, precipitated with ethanol and 2.5 ug of DNA were used for *in vitro* transcription (Promega). After DNAse treatment, the RNA was precipitated with ethanol. After resuspension in water, RNA integrity was checked by agarose electrophoresis treated or not with RNAse A. Chromatin extracts from *APOLO* RNAi plants were obtained as for ChIP and 1ug of each *in vitro* transcribed RNA was incubated separately with equal amounts of chromatin and 1μl of RNAseOUT (Invitrogen), for 45 min at 4 °C. Incubated samples were used for a regular DRIP-DNA, as explained above. Input samples were assessed also by RT-qPCR to check if transcript stability throughout the experiment was the same for both *APOLO* and *mutAPOLO*.

RNA Isolation by DNA Purification (RIDP)

For RNA isolation by DNA purification (RIDP), nuclei extracts were obtained as for ChIP, although without crosslinking. After soft sonication (3 cycles 30'' ON - 30'' OFF in the Diagenode Picoruptor), 200 μl of chromatin were treated for 45 min at 37 °C with 0.6 units of T5 exonuclease (NEB). The reaction was ended adding 2 μl of 1M EDTA and 10% of the volume was kept aside to use as Input samples. The rest of the volume was incubated 30 min at room temperature in rotation with 50 μl of Dynabeads MyOne Streptavidin C1 pre-coated with 2 μl of the corresponding 100 μM biotinylated probe. After incubation, the samples were washed 3 times with ChIRP Wash Buffer (see ChIRP Protocol). Finally, the beads were resuspended in 200 μl of RNA-se free water and RNA was purified using TRI Reagent (Sigma-Aldrich). RT and qPCR were performed as indicated above. The results were indicated as %INPUT. RNAseH treatment was used to demonstrate that *APOLO* interaction with its targets is mediated by R-loop formation. In parallel, RIDP was used to purify genomic DNA (gDNA) recovered with each biotinylated probe, compared with a non-associated biotinylated probe taken as a negative control. This last control was performed to demonstrate that specific DNA loci can by purified by RIDP.

GUS Staining and GFP Confocal Microcopy

Images acquisition and analysis were performed on the IPS2 Imaging Facility. *PID-APOLO* intergenic region was cloned in pKGWFS7 vector controlling the expression of the reporter genes *GFP* and *GUS*. GUS staining was performed as described previously (Manavella et al., 2008). Stained roots were observed under an AxioImager Z2 (Zeiss) equiped with Plan-Apochromat 40x/NA 1,4, DIC M27 US-VIS-IR oil immersion lens, using DIC contrast. The same intergenic region was also cloned in a pART27 derived vector where a rfa cassette and a *erGFP* cassette were introduced by cloning in the *Not*I site of the plasmid. Once homozygous, these line was crossed with the Dr5:erRFP reporter line as described by Marin et al. (2010).

Images of fluorescent proteins were obtained with LSM880 Zeiss confocal microscope equipped with LD C-Apochromat 40x/NA 1,1 W Korr M27 US-VIS-IR water immersion lens. erGFP and erRFP fluorescence were respectively excited with 488 and 561 nm argon laser line and emission recorded between 490-550 nm and 580-645 nm. Cell walls were stained as described by Musielak et al. (2015) with the optical brightener SCRI Renaissance 2200 and observed using 405 nm diode and recorded between 410 and 485 nm.

QUANTIFICATION AND STATISTICAL ANALYSIS

HiSeq reads from RNA-seq were first adaptor trimmed and then analyzed using the TopHat and Cufflinks software. TopHat v2.0.9 (Trapnell et al., 2009) was utilized for alignment of short reads to the *Arabidopsis* thaliana genome TAIR10, Cufflinks v2.2.0 (Trapnell et al., 2010) for transcript assembly and differential expression, and cummeRbund v2.0.0 for visualization of differential analysis. Default parameters (p value: 0.05; statistical correction: Benjamini Hochberg; FDR: 0.05) were used. For ChiRP-Seq, the libraries were sequenced on the Illumina Hiseq 2500 as single-end 50 base reads following Illumina's instructions. Sequence reads were quality controlled and adapter trimmed using FASTQC and trimmomatic. Sequenced reads were mapped to the reference genome *Arabidopsis*, TAIR10 using Bowtie (Langmead and Salzberg, 2012). Arguments to Bowtie are: -m 1 –strata –best -y -S -l 40 -p 2. Alignment statistics are provided in Table S5. Unique mapping strategy was adopted. To identify significantly enriched regions,

MACS2 was used with the following parameters: no_shift; Bandwidth:300; mfold of 5:30; q-value cutoff:0.05 (Zhang et al., 2008). Peak annotations based on proximity and overlap to genes were performed using HOMER (Heinz et al., 2010). Enrichment profile at TSS and along the genes were plotted using NGSplot (Shen et al., 2014).

For RT-qPCR, three independent biological samples were considered, each prepared from a pool of at least 10 individuals. Student t test was performed considering two-tailed samples of different variance. For Figures 1A and 3C qPCR was performed using 3 independent biological replicates for *35S:APOLO* samples and 2 for RNAi lines (each conformed by a pool of hundreds of individual seedlings). For Figures 1H, 2F, and S3B, the 3C approach was performed with 2 independent biological replicates from pools of *35S:APOLO1* and *2*, or *RNAi1* and *2*, respectively. For Figures 1G, 2E, and S3A, ChIRP was performed with 2 independent biological replicates from pools of *35S:APOLO1* and *2*, or *RNAi1* and *2*, respectively. The graphs were generated with the mean and SD of the EVEN samples, although the results were validated using the ODD samples in every case. Information of H3K27me3 for Figure 1B was taken directly from an integrated epigenome dataset previous published (Liu et al., 2016). RIDP in Figures 6D and S7B–S7D was performed with 3 biological replicates. R-loop information to generate the metagene distribution of Figure 3E was directly taken from Supplemental Table 3 in Xu et al. (2017). Analyses of the high resolution HiC (Liu et al., 2016) for interactions between *APOLO* targtes genomic bins are plotted using inhouse R scripts (Figures 3B and S4).

All DNA probes used for ChIRP, qPCR and cloning are included in Table S4.

Regulated genes in response to auxin were extracted from previous experiments (Bazin et al., 2018), where auxin regulated genes were identified as those having a condition effect in Col0 WT plants. Enrichment of auxin regulated genes was investigated using a hypergeometric test in R (v3.4.2).

DATA AND CODE AVAILABILITY

The ChIRP-Sequencing and RNA-sequencing datasets generated in this study are available at GEO with the accession code GSE117486 (https://www.ncbi.nlm.nih.gov/geo/query/acc.cgi?acc=GSE117486). Imaging raw data is available in Mendeley Data (https://dx.doi.org/10.17632/z4j5zn2wc7.1).